J|A|C|S ARTICLES

Published on Web 09/17/2010

Spatially and Size Selective Synthesis of Fe-Based Nanoparticles on Ordered Mesoporous Supports as Highly Active and Stable Catalysts for Ammonia Decomposition

An-Hui Lu,*[,†,‡] Joerg-Joachim Nitz,[†] Massimiliano Comotti,[†] Claudia Weidenthaler,[†] Klaus Schlichte,[†] Christian W. Lehmann,[†] Osamu Terasaki,[§,||] and Ferdi Schüth[†]

Max-Planck-Institut für Kohlenforschung, D-45470 Mülheim an der Ruhr, Germany, State Key Laboratory of Fine Chemicals, School of Chemical Engineering, Dalian University of Technology, Dalian 116012, China, and Structural Chemistry, Arrhenius Laboratory, Stockholm University, 10691 Stockholm, Sweden

Received June 17, 2010; E-mail: anhuilu@dlut.edu.cn

Abstract: Uniform and highly dispersed γ-Fe_2O_3 nanoparticles with a diameter of ~6 nm supported on CMK-5 carbons and C/SBA-15 composites were prepared via simple impregnation and thermal treatment. The nanostructures of these materials were characterized by XRD, Mössbauer spectroscopy, XPS, SEM, TEM, and nitrogen sorption. Due to the confinement effect of the mesoporous ordered matrices, γ-Fe_2O_3 nanoparticles were fully immobilized within the channels of the supports. Even at high Fe-loadings (up to about 12 wt %) on CMK-5 carbon no iron species were detected on the external surface of the carbon support by XPS analysis and electron microscopy. Fe_2O_3/CMK-5 showed the highest ammonia decomposition activity of all previously described Fe-based catalysts in this reaction. Complete ammonia decomposition was achieved at 700 °C and space velocities as high as 60 000 $cm^3\ g_{cat}^{-1}\ h^{-1}$. At a space velocity of 7500 $cm^3\ g_{cat}^{-1}\ h^{-1}$, complete ammonia conversion was maintained at 600 °C for 20 h. After the reaction, the immobilized γ-Fe_2O_3 nanoparticles were found to be converted to much smaller nanoparticles (γ-Fe_2O_3 and a small fraction of nitride), which were still embedded within the carbon matrix. The Fe_2O_3/CMK-5 catalyst is much more active than the benchmark NiO/Al_2O_3 catalyst at high space velocity, due to its highly developed mesoporosity. γ-Fe_2O_3 nanoparticles supported on carbon-silica composites are structurally much more stable over extended periods of time but less active than those supported on carbon. TEM observation reveals that iron-based nanoparticles penetrate through the carbon layer and then are anchored on the silica walls, thus preventing them from moving and sintering. In this way, the stability of the carbon-silica catalyst is improved. Comparison with the silica supported iron oxide catalyst reveals that the presence of a thin layer of carbon is essential for increased catalytic activity.

1. Introduction

Over the past decades the synthesis of solid catalysts with defined structure and homogeneously distributed and size selected particles supported on high surface area materials in a controlled manner has become possible.[1−4] However, the deposition of particles in predefined regions of a support material on the nanometer scale is still a challenge, while macroscopically this can be achieved, such as in the synthesis of egg-shell type catalysts.[5] Some reports have been published, such as the selective deposition of magnetic particles exclusively on the external surface of ordered mesoporous materials by a reversible pore-blocking strategy,[6,7] the controlled embedding of noble metal particles in the mesopores[8,9] and the micropores of ordered mesoporous silica,[10] or the targeted deposition of single catalytic particles in the core of hollow zirconia shells.[11]

A particularly suitable matrix for the spatially controlled deposition of catalytically active particles is CMK-5, an ordered mesoporous carbon with a dual pore system.[12] In conventional porous carbon materials, the pore system often consists of the

† Max-Planck-Institut für Kohlenforschung.
‡ Dalian University of Technology.
§ Stockholm University.
|| Current address: Graduate School of EEWS (WCU), KAIST, Daejeon 305-701, Republic of Korea.

(1) Somorjai, G. A.; Park, J. Y. *Angew. Chem., Int. Ed.* **2008**, *47*, 9212.
(2) Thomas, J. M.; Hernandez-Garrido, J. C.; Rajab, R.; Bellc, R. G. *Phys. Chem. Chem. Phys.* **2009**, *11*, 2799.
(3) Thomas, J. M.; Klinowski, J. *Angew. Chem., Int. Ed.* **2007**, *46*, 7160.
(4) Diesing, T.; Rojas, G.; Klapper, M.; Fink, G.; Müllen, K. *Angew. Chem., Int. Ed.* **2009**, *48*, 6472.
(5) Joo, S. H.; Park, J. Y.; Tsung, C.-K.; Yamada, Y.; Yang, P.; Somorjai, G. A. *Nat. Mater.* **2009**, *8*, 126.
(6) Lu, A.-H.; Li, W.-C.; Kiefer, A.; Schmidt, W.; Bill, E.; Fink, G.; Schüth, F. *J. Am. Chem. Soc.* **2004**, *126*, 8616.
(7) Lu, A.-H.; Schmidt, W.; Matoussevitch, N.; Bönnemann, H.; Spliethoff, B.; Tesche, B.; Bill, E.; Kiefer, W.; Schüth, F. *Angew. Chem., Int. Ed.* **2004**, *43*, 4303.
(8) Konya, Z.; Puntes, V. F.; Kiricsi, I.; Zhu, J.; Alivisatos, P.; Somorjai, G. A. *Catal. Lett.* **2002**, *81*, 137.
(9) Sun, J.; Ma, D.; Zhang, H.; Liu, X.; Han, X.; Bao, X.; Weinberg, G.; Pfaender, N.; Su, D. *J. Am. Chem. Soc.* **2006**, *128*, 15756.
(10) Yang, C.-M.; Zibrowius, B.; Spliethoff, B.; Schüth, F. *Chem. Mater.* **2007**, *19*, 3205.
(11) Arnal, P. M.; Comotti, M.; Schüth, F. *Angew. Chem., Int. Ed.* **2006**, *45*, 8224.
(12) Joo, S. H.; Choi, S. J.; Oh, I.; Kwak, J.; Liu, Z.; Terasaki, O.; Ryoo, R. *Nature* **2001**, *412*, 169.

 10.1021/ja105308e

available space between primary particles and, thus, is usually ill-defined. In such cases, one may anticipate an inhomogeneous distribution of the active species over the support material. Ordered nanostructured carbons, such as CMK-5, have pore systems with a defined narrow pore size distribution and tunable pore sizes. Thus, well-defined catalysts can be produced in a confining environment. The particle sizes of metal or metal oxide catalysts should remain equal to or smaller than the pore sizes of the supports due to the spatial limitations. In order to control not only particle sizes but also particle location in such materials, we developed a pathway for the targeted modification of only the intratubular pores of CMK-5 to create highly active catalysts for ammonia decomposition.

Liquid ammonia has recently been considered as a potential source for clean and carbon oxide free hydrogen.[13,14] Generating H_2 via ammonia decomposition has gained much attention because of the low cost of this technology and ease of operation compared to the complex systems required for reforming methanol or hydrocarbons. In the past, the NH_3 decomposition reaction has mainly been studied in order to obtain further insight into the reaction kinetics of NH_3 synthesis.[15,16] Nowadays, reports on the decomposition of NH_3 mainly focus on the generation of high quality H_2 to supply PEM fuel cells.[17] In comparison to other carbonaceous H_2 precursors such as methane or methanol, NH_3 offers a higher H_2 storage capacity (17.7 wt %) and a higher energy density (3000 W h/kg).[18,19] Moreover, at room temperature and at a pressure of 10 bar, NH_3 is in liquid form which makes the storage and delivery relatively easy. More importantly, H_2 generation from NH_3 does not produce any CO_x ($x = 1, 2$) as a byproduct, which is crucial for fuel cell applications. Using NH_3 as the hydrogen source, the problem of Pt catalyst poisoning can be avoided.[20,21] In addition, efficient ammonia decomposition also offers the possibility to remove ammonia from the product stream of coal gasification processes.[22] The cleanup of raw fuel gas produced in an integrated gasification combined cycle (IGCC) plant will increase the power generation efficiency and lead to a more efficient reduction of CO_2, compared to conventional coal fired power plants.

In the past decade, many different metals including Fe, Pd, Pt,[23] Ni,[24] Ru,[25] Ir,[26] and Co;[27] alloys including $Zr_{1-x}Ti_xM_1M_2$ with $M_1, M_2 =$ Cr, Mn, Fe, Co, Ni and $x = 0-1$;[28] and nitrides[29] and carbides[30,31] including MON_x, VN_x, VC_x, and MoC_x have been tested as catalysts for ammonia decomposition. Among the systems studied so far, Ru-based catalysts showed the highest activity in ammonia decomposition.[25] However, such catalysts have the obvious disadvantages of high cost and limited availability, especially of Ru, for large scale applications. Fe- or Ni-based catalysts also exhibit good activity in ammonia decomposition though they usually work at higher temperatures than ruthenium based materials. The activity of the catalysts is also highly dependent on the nature of the support materials.[32,33] Among the widely investigated supports in ammonia decomposition, such as carbon, silica, and alumina,[23,26] carbon materials with their high thermal stability and electrical conductivity are advantageous in high temperature reactions and are thought to be able to transfer electrons from the support to the active species, thus facilitating the recombinative desorption of surface nitrogen atoms. Li and co-workers have demonstrated that Ru catalysts supported on various carbon supports, such as graphitic carbon, carbon black, and CMK-3 carbons, are active in ammonia decomposition.[34] The most active catalyst consists of small Ru nanoparticles with sizes of ca. 3−4 nm and a graphitized carbon support.

In this study, γ-Fe_2O_3 nanoparticles were immobilized within one of the pore systems of CMK-5 carbons and a carbon-SBA-15 composite by impregnation, drying, and calcination.[35,36] This γ-Fe_2O_3/CMK-5 material showed the highest ammonia decomposition activity of all previously reported Fe-based catalysts. Moreover, notably Fe_2O_3-carbon-SBA-15 catalysts are very stable over extended reaction times. The excellent performance is attributed to the spatial confinement in the pores and the strong interaction with the silica in the composite support, preventing nanoparticle migration and subsequent sintering.

2. Experimental Section

2.1. Synthesis of SBA-15 Template. Hexagonally ordered SBA-15 mesoporous silica was synthesized according to the synthesis conditions reported by Zhao et al.[37] In a typical synthesis, SBA-15 was prepared using 10.0 g of Pluronic P123 ($EO_{20}PO_{70}EO_{20}$, Sigma Aldrich) dissolved in 262.5 mL of demineralized H_2O and 50 mL of HCl (37%). After complete dissolution, 21.3 g of tetraethoxysilane (TEOS, Acros 99%) were added dropwise (80 mL h^{-1}) under constant vigorous stirring at a temperature of 40 °C. The stirring was continued for another 6 h at the same temperature. Afterward the white milky suspension was transferred into an autoclave and placed under static conditions at 110 °C in an oven for 3 days. The obtained silica product was directly filtered without further washing, dried at 90 °C, and then calcined in air at a temperature of 550 °C for 6 h with a heating rate of 4 °C min^{-1}.

2.2. Synthesis of CMK-5 Carbon. Tubular mesoporous CMK-5 type carbon was synthesized via a surface-templating approach as described in our previous report.[38] In a typical synthesis, furfuryl alcohol (FA, Fluka, 98%) as a carbon precursor was dissolved in

(13) Chellappa, A. S.; Fischer, C. M.; Thomson, W. J. *Appl. Catal., A* **2002**, *227*, 231.
(14) Yin, S. F.; Xu, X. P.; Au, C. T. *Appl. Catal., A* **2004**, *277*, 1.
(15) Ertl, G.; Huber, M. *J. Catal.* **1980**, *61*, 537.
(16) Hashimoto, K.; Toukai, N. *J. Mol. Catal. A* **2000**, *161*, 171.
(17) Choudhary, T. V.; Goodman, D. W. *J. Catal.* **2000**, *192*, 316.
(18) Metkemeijer, R.; Achard, P. *Int. J. Hydrogen Energy* **1994**, *19*, 535.
(19) Metkemeijer, R.; Ahard, P. *Power Sources* **1994**, *49*, 271.
(20) Li, X. K.; Ji, W. J.; Zhao, J.; Wang, S. J.; Au, C. T. *J. Catal.* **2005**, *236*, 181.
(21) Armor, J. N. *Appl. Catal., A* **1999**, *176*, 159.
(22) Mojtahedi, W.; Abbasian, J. *Fuel* **1995**, *74*, 1698.
(23) Yin, S. F.; Zhang, Q. H.; Xu, B. Q.; Zhu, W. X.; Ng, C. F.; Au, C. T. *J. Catal.* **2004**, *224*, 384.
(24) Abashar, M. E. E.; Al-Sughair, Y. S.; Al-Mutaz, I. S. *Appl. Catal., A* **2002**, *236*, 35.
(25) Zheng, W.; Zhang, J.; Xu, H.; Li, W. *Catal. Lett.* **2007**, *119*, 311.
(26) Choudhary, T. V.; Svadinaragana, C.; Goddman, D. W. *Catal. Lett.* **2001**, *72*, 197.
(27) Terrones, M.; Grobert, N.; Olivares, J.; Zhang, J. P.; Terrones, H.; Kordatos, K.; Hsu, W. K.; Hare, J. P.; Townsend, P. D.; Prassides, K.; Cheetham, A. K.; Kroto, H. W.; Walton, D. R. M. *Nature* **1997**, *388*, 52.
(28) Boffito, C.; Baker, J. D. WO Patent 9840311, 2002.
(29) Boisen, A.; Dahl, S.; Nørskov, J. K.; Christensen, C. H. *J. Catal.* **2005**, *230*, 309.
(30) Choi, J.-G.; Ha, J.; Hong, J. W. *Appl. Catal., A* **1998**, *168*, 47.
(31) Choi, J.-G. *J. Catal.* **1999**, *182*, 104.
(32) Yin, S. F.; Xu, B. Q.; Ng, C. F.; Au, C. T. *Appl. Catal., B* **2004**, *48*, 237.
(33) Szmigiel, D.; Raróg-Pilecka, W.; Miśkiewicz, E.; Gliñski, M.; Kielak, M.; Kaszkur, M.; Kowalcyk, Z. *Appl. Catal., A* **2004**, *273*, 105.
(34) Li, L.; Zhu, Z. H.; Yan, Z. F.; Lu, G. Q.; Rintoul, L. *Appl. Catal., A* **2007**, *320*, 166.
(35) Lu, A.-H.; Li, W.-C.; Hou, Z.; Schüth, F. *Chem. Commun.* **2007**, 1038.
(36) Zheng, W.; Zhang, J.; Xu, H.; Li, W. *Catal. Lett.* **2007**, *119*, 311.
(37) Zhao, D. Y.; Feng, J.; Huo, Q.; Melosh, N.; Frederickson, G. H.; Chmelka, B. F.; Stucky, G. D. *Science* **1998**, *279*, 548.
(38) Lu, A.-H.; Li, W.-C.; Schmidt, W.; Kiefer, W.; Schüth, F. *Carbon* **2004**, *42*, 2939.

Scheme 1. Illustration of the Synthesis Principle of γ-Fe_2O_3 Nanoparticles Spatially Confined within the Tubes of CMK-5 Carbon

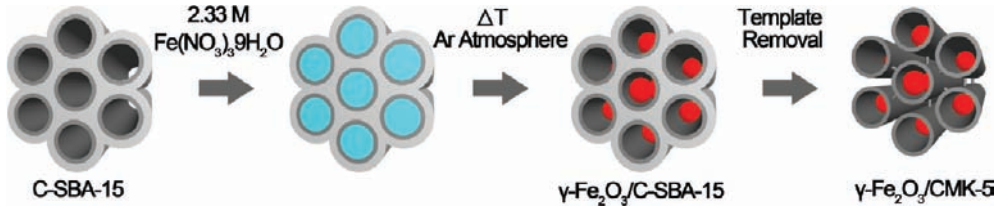

trimethylbenzene (TMB, Aldrich, 99%), and oxalic acid (OA, Acros, 98%) was added as a polymerization catalyst. To obtain tubular carbon, the volume ratio between FA and TMB was fixed to 1:1. This solution was infiltrated at room temperature into the free pore space of SBA-15. After polymerization at 50 °C for 1 day and then at 90 °C for 2 days under air, the composite materials were treated under an argon atmosphere at 150 °C for 4 h and then heated to 300 °C with a heating rate of 1 °C min^{-1} and finally to 850 °C for 4 h with a heating rate of 5 °C min^{-1}. The obtained black carbon-silica composites, named as CS, were transferred to an aqueous-ethanolic NaOH (1.5 M) solution to leach out the silica. After filtration and washing with distilled H_2O, dilute $HNO_{3(aq)}$, and acetone, the obtained black powder was dried at 90 °C to obtain high quality CMK-5.

2.3. Synthesis of Well-Defined γ-Fe_2O_3 Supported Catalysts. CMK-5 carbon has a bimodal pore system, which is derived from surface-templating the inner pores of SBA-15 and silica leaching, respectively. To selectively immobilize Fe_2O_3 within the tubes of CMK-5 carbons and leave the mesopores between the tubes open, the iron precursor was impregnated into the carbon-silica composite (CS), because here only the pores within the tubes are accessible. The preparation procedure is illustrated in Scheme 1. First, 2.33 M $Fe(NO_3)_3 \cdot 9H_2O$ containing one drop of HCl (37%) was impregnated into the pore space of CS. Subsequently, the samples were dried at room temperature and further heated to temperatures up to 1000 °C with a heating rate of 2 °C min^{-1} and left at this temperature for 4 h in an argon atmosphere. Finally the silica was leached out by an aqueous NaOH solution. The resulting γ-Fe_2O_3/CMK-5 catalyst was recovered by filtration and washed with demineralized water and acetone. Catalysts with different Fe_2O_3 loadings were synthesized by diluting the stock solution by a factor of 2, 4, 5, 6, and 8. Catalysts are labeled as C-Fe-z-β where z and β indicate the molarity of the aqueous $Fe(NO_3)_3$ solution and the thermal treatment temperature, respectively. Similarly, Fe_2O_3 supported on CS was named CS-Fe-z-β.

2.4. Characterization. The X-ray diffraction patterns of all samples were measured on a STADI P diffractometer (STOE) in Bragg−Brentano (reflection) geometry using Cu Kα radiation. To avoid possible interfering reflections from stainless steel holders, for selected samples also a quartz holder was used. Transmission electron micrographs (TEM) were obtained using a Hitachi HF 2000 microscope (operated at 200 kV), Hitachi H-7500 (operated at 100 kV), and JEOL 3010 (operated at 300 kV). In order to better analyze the dispersion and the sizes of the iron oxide nanoparticles, catalysts were embedded in Spurr's resin and cut into 60 nm thin sections using a microtome. High resolution scanning electron micrographs were recorded using a Hitachi S-5500 instrument. Nitrogen sorption isotherms were measured with an ASAP2010 adsorption analyzer (Micromeritics) at liquid nitrogen temperature (77 K). Prior to the measurements the samples were degassed at 150 °C for a minimum of 4 h. The surface area was calculated by the BET method, typically using the points in the pressure range from $p/p_0 = 0.04-0.2$. The total pore volume was estimated from the amount of nitrogen adsorbed at $p/p_0 \cong 0.99$. Pore size distribution curves were obtained using the BJH method from the adsorption branch (to avoid misinterpretation due to network percolations effects). XPS measurements were performed with a Kratos HSi spectrometer with a hemispherical analyzer. The monochromatized Al Kα X-ray source ($E = 1486.6$ eV) was operated at 15 kV and 15 mA. For the narrow scans, an analyzer pass energy of 40 eV was applied. The hybrid mode was used as the lens mode. The base pressure in the analysis chamber during the experiments was 4×10^{-7} Pa. To account for charging effects, all spectra are referred to C 1s at 284.5 eV. Mössbauer spectra were collected on a ^{57}Fe Mössbauer spectrometer. The samples were measured at room temperature. Mössbauer data were recorded on a spectrometer with alternating constant acceleration. The minimum experimental line width was 0.24 mm s^{-1} (full width at half-height). The sample temperature was maintained as constant either in an Oxford Instruments Variox or an Oxford Instruments Mössbauer-Spectromag cryostat. The latter was a split-pair superconducting magnet system for applied fields up to 8 T where the temperature of the sample can be varied in the range 1.5−250 K. The field at the sample was perpendicular to the γ-beam. The ^{57}Co/Rh source (1.8 GBq) was positioned at room temperature inside the gap of the magnet system at a zero-field position. Isomer shifts were quoted relative to iron metal at 300 K.

2.5. Catalytic Test. Catalytic activities were evaluated in a quartz tube fixed bed reactor. In a standard experiment, 25 mg of catalyst (as powder) were placed on a frit in the reactor, and the temperature was raised in a pure ammonia stream (25 cm^3 min^{-1} at 1.15 bar, corresponding to a space velocity of 60 000 cm^3 g_{cat}^{-1} h^{-1}) with a heating rate of 10 °C min^{-1} up to 600 °C. This temperature was maintained for 20 h, and the catalytic activity was recorded over this time in order to evaluate the stability of the catalyst. After the stability test, the temperature was varied between 400 and 700 °C at a space velocity of 60 000 cm^3 g_{cat}^{-1} h^{-1}. In some cases the space velocity was varied between 7500 and 120 000 cm^3 g_{cat}^{-1} h^{-1} by changing the ammonia flow in order to determine the dependence of conversion on the temperatures and flow rates. Outlet gases (N_2, H_2, and NH_3) were analyzed under isothermal conditions by an online gas chromatograph (3000A MicroGC, Agilent), equipped with two lines: the first one equipped with a PLOTU precolumn/Molsieve column in combination with Ar as a carrier gas for N_2, H_2, and CH_4 separation and quantification, the second equipped with a PLOTU column with He as a carrier gas for NH_3 quantification. Both lines are equipped with TCD detectors.

3. Results and Discussion

3.1. Location and Crystal Phase Identification of Iron Oxides Confined in CMK-5. The crystal phases of the iron oxides could be important for the activity in ammonia decomposition. Thus, the dependence of phase composition of the iron oxides within the support on temperature was investigated.[39] First, CS composites were impregnated with 2.33 M $Fe(NO_3)_3$ solution and then heated to different temperatures from 200 to 900 °C under argon. After removal of silica, the crystal phases of the samples C-Fe-2.33-β were characterized by XRD, Mössbauer spectroscopy, and TEM. XRD patterns (Figure 1A) were measured routinely on a stainless steel holder which shows the reflections of metallic iron. For comparison, some selected samples were measured on a quartz holder (Figure 1B). In none of the XRD patterns measured on a quartz holder were

(39) Jedynak, A.; Kowalczyk, Z.; Szmigiel, D.; Raróg, W.; Zieliński, J. *Appl. Catal., A* **2002**, *237*, 223.

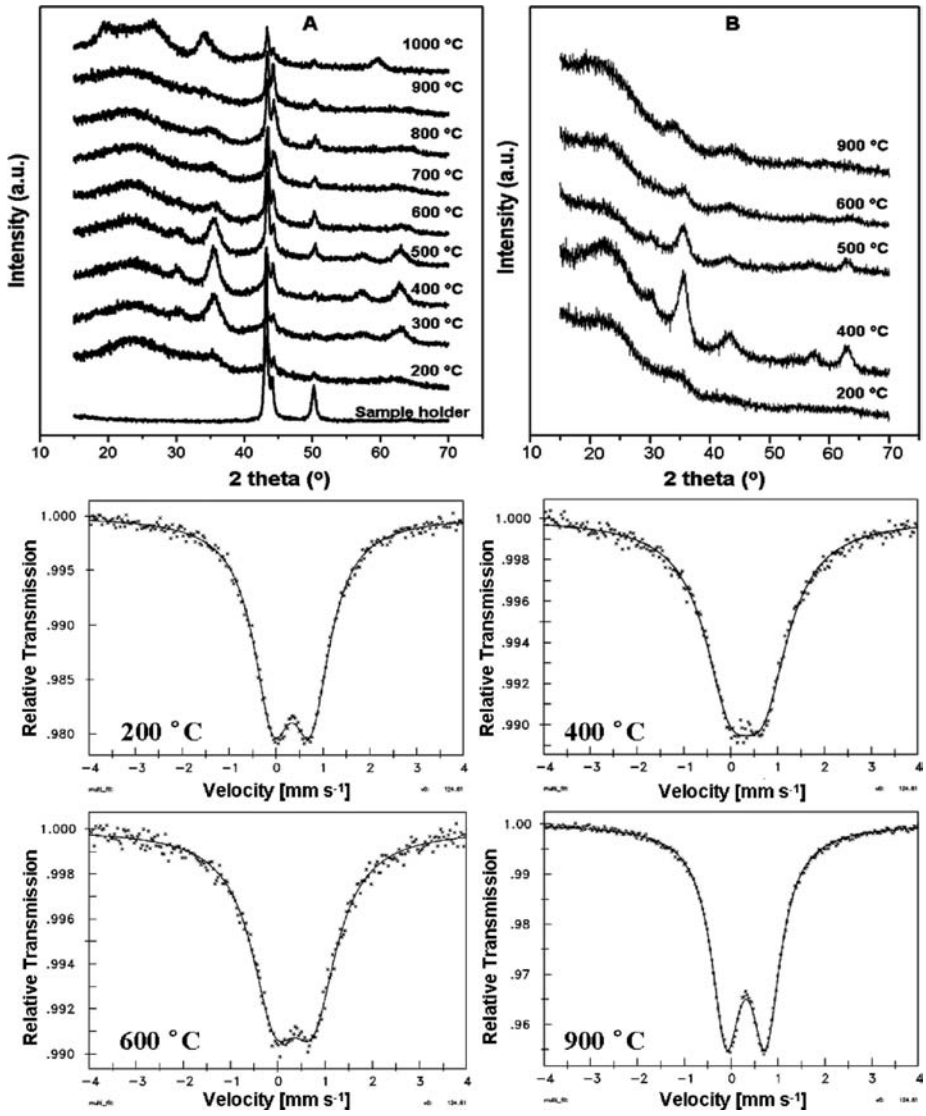

Figure 1. XRD patterns ((A) measured on a stainless steel holder; (B) measured on a quartz holder) and room temperature measured ^{57}Fe Mössbauer spectra of C-Fe-2.33-β (β: calcination temperature) prepared at different temperatures.

reflections of metallic iron detected. All reflections observed were strongly broadened, irrespective of the phase, indicating the existence of very small crystals. In the temperature range between 200 and 400 °C, the reflection intensities corresponding to γ-Fe_2O_3 increase with temperature. Based on the XRD patterns, the mean size of the γ-Fe_2O_3 crystallites is in the range of 4−6 nm as calculated by the Scherrer formula. When the temperature exceeds 400 °C, the intensities of the reflections decrease and reflections at ∼36° 2θ shift to lower angles, indicating that a phase transformation of the iron oxides occurs. At temperatures higher than 600 °C, the crystalline γ-Fe_2O_3 is clearly transformed to other iron containing compound, most likely present as amorphous compounds or nanosized particles, which is indicated by the overall decrease of reflection intensity.

In the case of small nanoparticles, it is difficult to distinguish between the γ-Fe_2O_3 and Fe_3O_4 phases based only on XRD analysis. To determine the oxidation state of iron, ^{57}Fe Mössbauer spectra were measured at room temperature. As shown in Table 1 all samples show very similar results: the isomer shift (δ) is in the range between 0.32 and 0.34 mm s^{-1} and the quadrupole splitting (Δ) is in the range between 0.74 and 0.84 mm s^{-1}, indicating in all cases a high spin Fe^{3+} material that is in good agreement with the literature for γ-Fe_2O_3.[40] Only the experimental peak width W (full width at half-maximum, fwhm) differs marginally. Since no Fe with a valence state of +2 was detected, the presence of the spinel phases of Fe_3O_4 or FeO at significant concentrations can be excluded. This indicates that, even in the presence of a thin layer of carbon, the Fe^{3+} cannot be reduced to Fe^{2+} or Fe under an inert atmosphere. Very interestingly, at low temperature and in the confined environment, magnetic γ-Fe_2O_3 rather than α-Fe_2O_3 is preferentially generated.

Table 1. Mössbauer Parameters of the C-Fe-2.33-β Series Samples

Sample	Isomer shift δ (mm s^{-1})	Quadrupole Splitting Δ (mm s^{-1})	Peak width W (mm s^{-1})
C-Fe-2.33-200	0.34	0.82	1.00
C-Fe-2.33-400	0.34	0.74	1.31
C-Fe-2.33-600	0.34	0.83	1.21
C-Fe-2.33-900	0.32	0.84	0.77

The results discussed above reveal that thermal treatment at 400 °C is adequate to completely decompose and convert

(40) Kuzmann, E. *Pure Appl. Chem.* **2003**, *75*, 801.

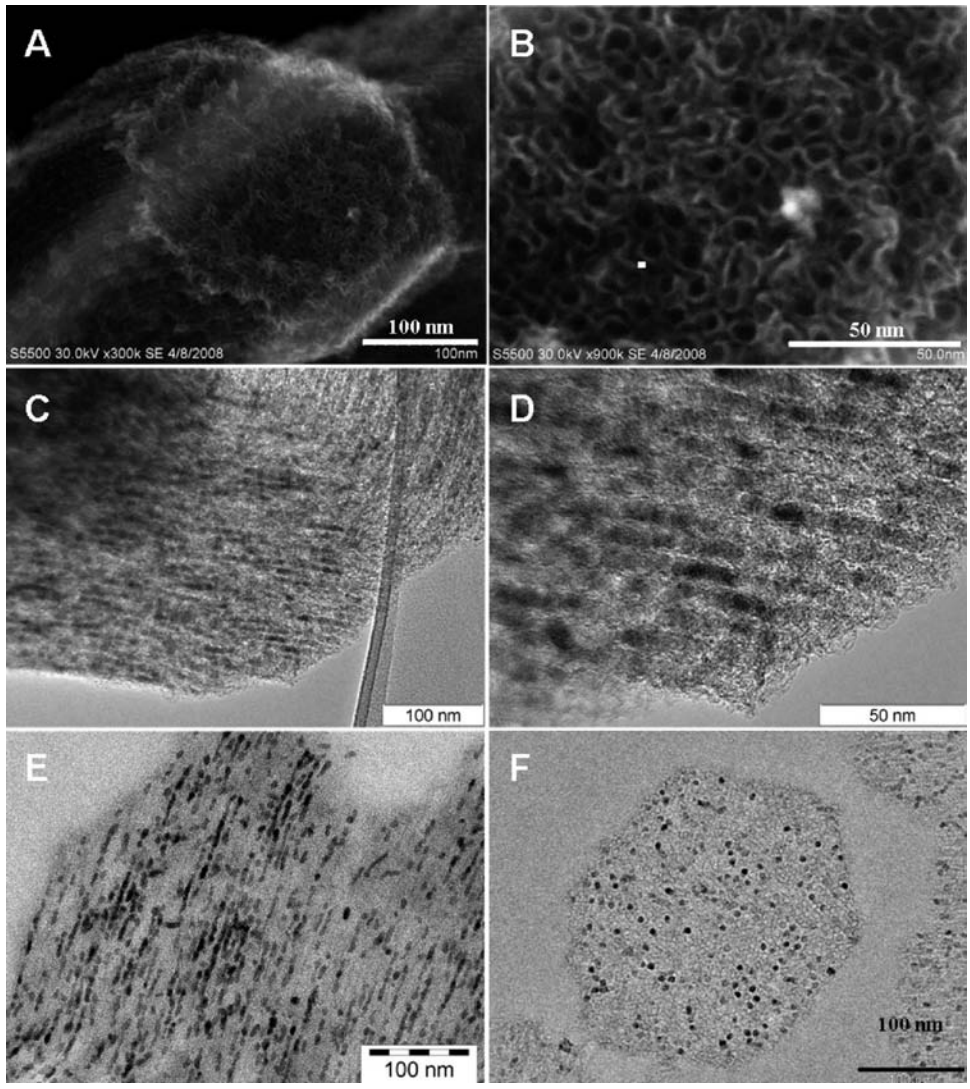

Figure 2. SEM (Hitachi S-5500) images (A, B) of CMK-5 carbon, and TEM images ((C, D) bulk material measured with Hitachi HF 2000; (E, F) 60 nm thin microtome sections measured with JEOL 3010) of C-Fe-2.33-400. The γ-Fe_2O_3 nanoparticles are deposited exclusively inside the inner pore system of the CMK-5 matrix.

$Fe(NO_3)_3$ to γ-Fe_2O_3 nanoparticles, without formation of other phases. In order to obtain a better understanding of the morphology and spatial arrangement of the components of this catalyst, first the catalyst support CMK-5 was investigated with HR-SEM. As can be seen in Figure 2A, B, CMK-5 essentially replicates the morphology of the mother template SBA-15. No excess amount of nonstructured carbon residue was observed on the replica. The two pore systems of CMK-5 can clearly be observed with unprecedented resolution in this SEM image. One can easily distinguish the tube-like mesopores and the pores generated by removal of the hard template. The diameters of the carbon tubes are about 6 nm, which is in good agreement with TEM and nitrogen sorption data mentioned below. The voids in between the carbon tubes, opened by leaching of the silica, have diameters of approximately 2−3 nm. The shape of these pores is not well-defined. Introducing the Fe_2O_3 particles into the carbon tubes does not lead to any changes in the HR-SEM images (not shown, but similar to that of Figure 2A, B), giving a first indication that the iron oxide particles are completely located inside the channel system. Sample C-Fe-2.33-400 was then characterized by TEM in order to examine the morphology and distribution of the supported γ-Fe_2O_3 particles. γ-Fe_2O_3 nanoparticles appear as elongated shapes and are homogeneously distributed in the intratubular pores of the CMK-5 support (Figure 2C, D). As expected from the synthetic procedure, the iron oxide is exclusively located within the carbon tubes, not in the pore space which has been created by removal of the silica. Even at such a high Fe-loading (12 wt %, see Table 2), no Fe_2O_3 nanoparticles are observed on the external surface of the carbon matrix, corroborating the HR-SEM data. To analyze more clearly the nanoparticle distribution, the resin embedded and cut C-Fe-2.33-400 samples were carefully characterized with TEM. As shown in Figure 2E, the image taken along the mesopore channels displays a high number of rod-type iron oxide particles highly dispersed within the mesopores. Figure 2F clearly shows the hexagonal arrangement of pores in CMK-5, and the black dots with sizes of around 6 nm are Fe_2O_3 particles that are exclusively embedded in the mesopores (inner tubes) of CMK-5. This result is in agreement with the size analysis from reflection broadening in the XRD. Careful analysis of many areas of this sample proved that no larger domains of Fe_2O_3 particles are located on the external surface of the carbon support, indicating that all the nanoparticles are selectively embedded in the inner pore system of CMK-5.

Table 2. EDX Mapping Results of the Fe-Loaded Catalysts

Sample	C (wt %)	Si (wt %)	O (wt %)	Fe (wt %)
CS-Fe-2.33-400	34.7	23.2	37.0	5.1
CS-Fe-1.17-400	35.8	25.4	36.3	2.5
CS-Fe-0.58-400	36.7	25.8	36.1	1.4
CS-Fe-0.47-400	35.4	25.0	34.2	1.2
CS-Fe-0.39-400	35.5	25.1	34.1	1.1
CS-Fe-0.29-400	37.4	26.5	35.3	0.8
CS-Fe-0.15-400	37.5	27.0	35.1	0.4
C-Fe-2.33-400	71.5	0.8	14.5	12.2
C-Fe-1.17-400	81.4	0.8	11.7	5.2
C-Fe-0.58-400	81.5	1.0	13.6	2.8
C-Fe-0.29-400	83.7	1.0	12.9	1.2

As discussed above, when the annealing temperature is higher than 600 °C, γ-Fe_2O_3 is subjected to phase transformation to other compounds. A representative example is C-Fe-2.33-900 which was treated at 900 °C. TEM analysis (Figure 3) shows that the particles are still homogeneously distributed over the carbon support. However, some big particles are now located on the external surfaces and the boundary of the carbon particles. At such temperatures, the Fe_2O_3 nanoparticles obviously become mobile and can thus leave the confinement of the mesopores. Further EDX (Hitachi HF 2000) analyses on these big particles reveal that they consist of iron and silicon at a molar ratio of 1:1. The nature of this material is unclear. One may expect amorphous or nanocrystalline iron silicates, but for most iron silicates one would expect the presence of Fe^{2+} which is not detected in the Mössbauer spectra. Thus, the amount of this phase either is below the detection limit or is not a conventional iron silicate.

In the following discussion, the influence of the amount of Fe-loading on the catalytic activity of the catalysts will be discussed. Catalysts with different Fe-loadings were prepared by impregnating aqueous solutions of $Fe(NO_3)_3$ having different nitrate concentrations into the mesopores of CS, followed by thermal treatment at 400 °C and the silica leaching step. EDX mapping analyses (Hitachi S-3500N) on these catalysts before and after silica leaching were performed. The EDX results are summarized in Table 2. All EDX mapping results confirm that, independently of the Fe_2O_3-loading, the immobilized γ-Fe_2O_3 particles are uniformly distributed over the support. Fe-loadings from 1.2 wt % to 12 wt % can be achieved easily by varying the concentration of $Fe(NO_3)_3$ solution via a single impregnation step. After NaOH solution leaching, the detected residual Si content is $\leq$1 wt %.

Differing from EDX analyses, XPS analysis is a surface sensitive technique with a sampling volume that extends from the surface to a depth of 1−5 nm.[41] XPS analysis of C-Fe-2.33-400 was performed in order to quantitatively determine the surface composition. The XPS result (Figure 4) shows that the C and O contents are about 97 and 3 wt %. The surface and near-surface concentration of iron is below or just at the detection limit. Resynthesis of a nominally identical sample gave

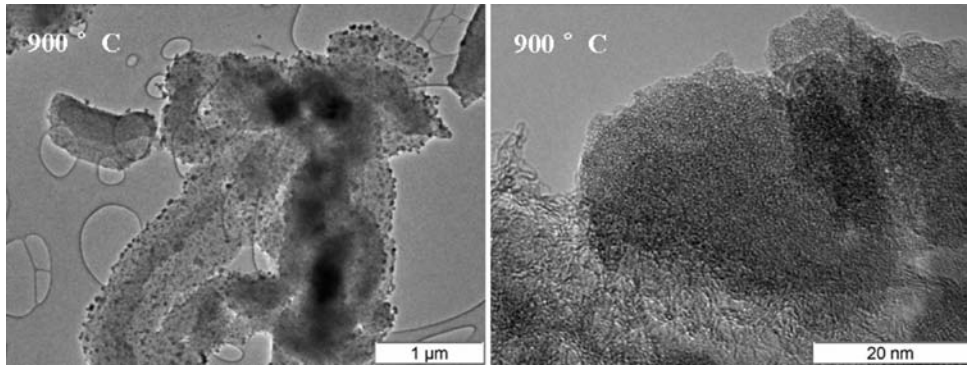

Figure 3. TEM (Hitachi HF 2000) images of C-Fe-2.33-900.

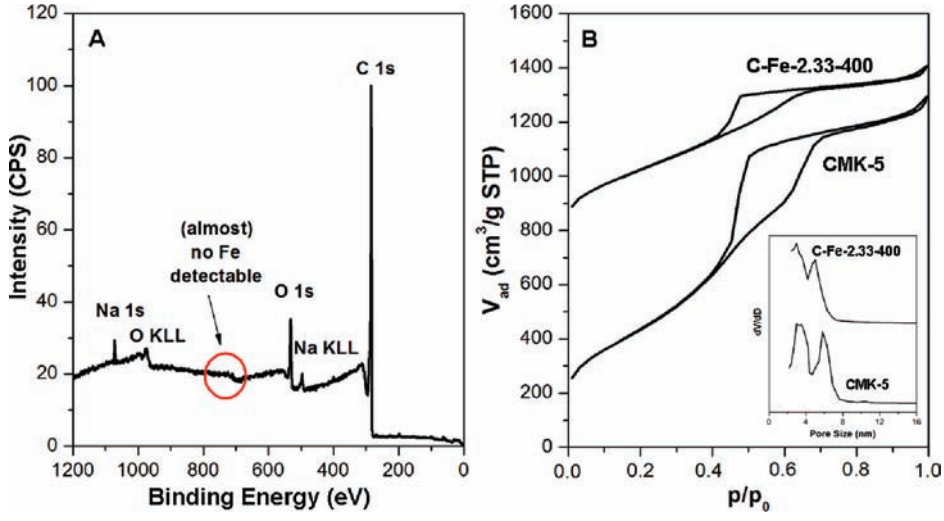

Figure 4. XPS survey scan (A) of C-Fe-2.33-400 and Nitrogen sorption isotherms (B; inset: pore size distributions) of C-Fe-2.33-400 and CMK-5. For clarity, the isotherm of C-Fe-2.33-400 is offset vertically by 650 cm^3 g^{-1} STP.

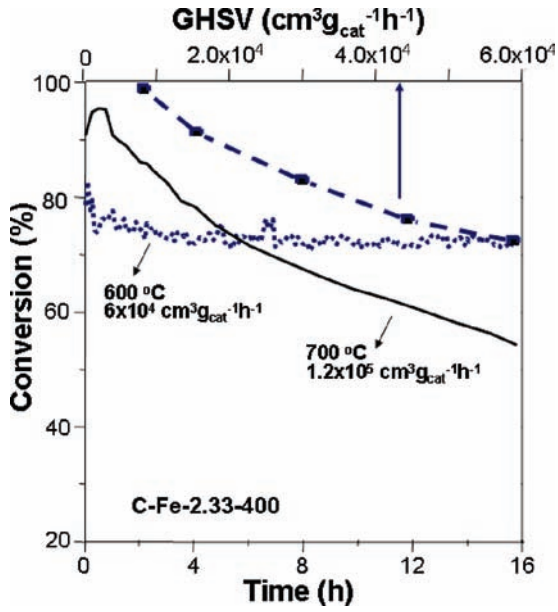

Figure 5. Catalytic activity measured at 600 °C as a function of GHSV for C-Fe-2.33-400, and catalyst stability measured both at 600 °C and GHSV = 60 000 $cm^3\ g_{cat}^{-1}\ h^{-1}$ (dotted line) and at 700 °C and GHSV = 120 000 $cm^3\ g_{cat}^{-1}\ h^{-1}$ (solid line).

the same result. This indicates that the Fe_2O_3 nanoparticles are exclusively immobilized in the pore system, confirming the previous conclusion from the electron microscopy analysis. This is in contrast to previously reported results on Fe/carbon nanotube catalysts where only ~85% of the Fe-nanoparticles were encapsulated within the carbon nanotubes.[42,43]

Figure 4 shows the nitrogen sorption isotherms of the original CMK-5 carbon and sample C-Fe-2.33-400 (loaded with γ-Fe_2O_3). They are of type IV with hysteresis loops in the relative pressure range of $p/p_0 = 0.4-0.7$. The pore size distributions of both materials calculated by the BJH method show a bimodal pore system, indicating that the pore structure of the carbon support is well-preserved after immobilization of γ-Fe_2O_3 nanoparticles. The specific surface area and pore volume of the iron oxide loaded sample are 1177 $m^2\ g^{-1}$ and 1.04 $cm^3\ g^{-1}$, which are substantially reduced compared to those (surface area and pore volume are 1783 $m^2\ g^{-1}$ and 2.18 $cm^3\ g^{-1}$) of the native CMK-5. This not only can be explained by the additional mass of the iron oxide (12.1 wt %) but also is probably related to blockage of part of the pore system, as can also be inferred from the electron microscopy data.

3.2. Ammonia Decomposition Reaction. Using sample C-Fe-2.33-400 as the catalyst, complete ammonia decomposition was achieved at 700 °C at a space velocity as high as 60 000 $cm^3\ g_{cat}^{-1}\ h^{-1}$ (Figure 5). Even at twice the space velocity (120 000 $cm^3\ g_{cat}^{-1}\ h^{-1}$) initially more than 90% of the ammonia can be converted. To the best of our knowledge, this is the best reported catalytic activity of Fe-based catalysts for this reaction. For example, Fe-containing carbon nanotubes convert only ~75% ammonia at a space velocity of 5000 $cm^3\ g_{cat}^{-1}\ h^{-1}$ and at 700 °C.[44]

Unfortunately, at such high temperatures, the C-Fe-2.33-400 catalyst deactivated quickly. After 16 h under an ammonia stream the conversion decreased to less than 60% at a space velocity of 120 000 $cm^3\ g_{cat}^{-1}\ h^{-1}$. However, at 600 °C, the C-Fe-2.33-400 catalyst is stable for 16 h on stream after a slight initial deactivation. At a space velocity of 60 000 $cm^3\ g_{cat}^{-1}\ h^{-1}$ the conversion remains constant at 74%. At this temperature, complete ammonia conversion to nitrogen and hydrogen was achieved at a space velocity of 7500 $cm^3\ g_{cat}^{-1}\ h^{-1}$. No methane, which could be a possible byproduct from methanation of the carbon support, was detected by GC in any run. The specific surface area of this catalyst changed from 1177 $m^2\ g^{-1}$ before reaction to 1378 $m^2\ g^{-1}$ after reaction.

For comparison, the commercial benchmark NiO/Al_2O_3 catalyst was tested under the same reaction conditions. As shown in Figure 6A, at 600 °C and a space velocity of 7500 $cm^3\ g_{cat}^{-1}\ h^{-1}$, about 73−79% of ammonia can be converted by the benchmark NiO/Al_2O_3 catalyst. At 600 °C, with an increase in space velocity from 7500 $cm^3\ g_{cat}^{-1}\ h^{-1}$ to 60 000 $cm^3\ g_{cat}^{-1}\ h^{-1}$, the conversion decreased from 76% to 29%. The performance of the C-Fe-2.33-400 catalyst is thus substantially better. The temperature dependent catalytic activity of the NiO/Al_2O_3 benchmark catalyst is shown in Figure 6B. It can be seen that, at a space velocity of 7500 $cm^3\ g_{cat}^{-1}\ h^{-1}$, the ammonia

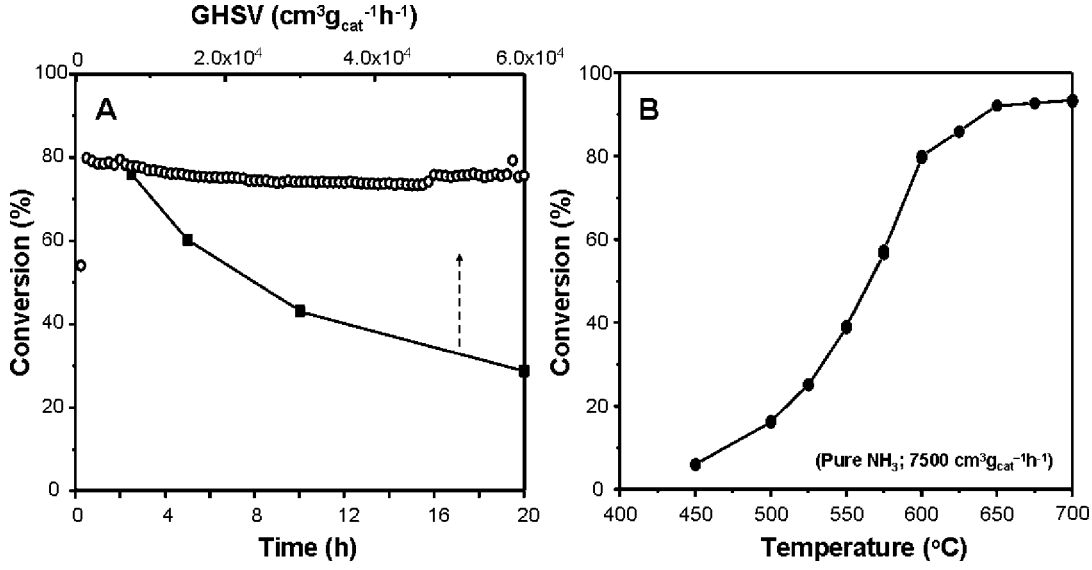

Figure 6. (A) Catalytic activity of the NiO/Al_2O_3 benchmark catalyst measured at 600 °C as a function of GHSV and the catalytic stability measured at 600 °C and GHSV = 7500 $cm^3\ g_{cat}^{-1}\ h^{-1}$; (B) temperature dependent catalytic activity measured at GHSV = 7500 $cm^3\ g_{cat}^{-1}\ h^{-1}$.

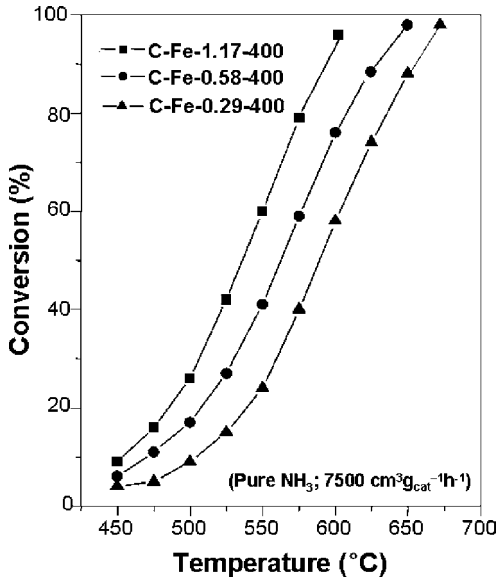

Figure 7. Catalytic activity measured at a GHSV of 7500 $cm^3\ g_{cat}^{-1}\ h^{-1}$ as a function of temperature for different Fe_2O_3/CMK-5 materials.

conversion increases from 6% at 450 °C to 93% at 700 °C. At 600 °C, only 80% of ammonia was converted, while over C-Fe-2.33-400 complete ammonia conversion is reached.

Furthermore, the influence of the Fe-loading on the catalytic activity of Fe_2O_3/CMK-5 catalysts was investigated. All catalysts, after a short activation period, reach a steady state conversion that is stable without any appreciable deactivation over the course of the experiments up to the final temperatures. As can be seen in Figure 7, the activity of Fe_2O_3/CMK-5 catalysts increases with increasing Fe-loading. Catalyst C-Fe-1.17-400 (5.2 wt % Fe) nearly completely decomposes ammonia at 600 °C, which is similar to the case of C-Fe-2.33-400. The other two catalysts showed complete ammonia decomposition at temperatures of 650 and 675 °C, respectively. After catalysis, these catalysts exhibited a mass loss of ca. 10 wt %.

To understand the deactivation of the catalysts under reaction conditions, the catalyst was collected after 16 h on stream and characterized by TEM and XRD. As seen in the TEM images (Figure 8A, B) of a catalyst taken after 16 h on stream at 600 °C, the iron oxide particles are still homogeneously distributed and embedded in the carbon matrix. Though the particles have grown to a small extent, they most likely still consist of very small crystals, as revealed by the XRD characterization (see below). This could be responsible for the slight initial deactivation. In contrast, big particles were observed after the sample had been exposed to the higher reaction temperature of 700 °C (Figure 8C, D). Some of the particles even have sizes exceeding 50 nm. Possibly, the initial 6 nm γ-Fe_2O_3 particles become mobile at high temperature and form larger particles through migration along the channels and penetration through the carbon walls of the carbon support. By carefully checking the boundary of the carbon matrix, no iron-based particles located on the external surface were observed. That is significantly different from the CS-Fe-2.33-900 shown in Figure 3. This indicates that although the iron oxide particles had sintered strongly they were most likely still embedded in the carbon matrix. Such a growth of particles within a porous matrix is also known from noble metals in zeolites, where the framework is locally destroyed to allow growth of particles exceeding the sizes of the structural voids.[45] The loss of the catalytic activity can thus be attributed to the formation of larger particles with a lower surface to volume ratio. Particle growth by sintering is dependent not only on temperature but also on other factors, such as texture, size, morphology, and the melting point of the particles. The so-called Tamman and Hüttig temperatures, which are directly correlated with the melting point, are good indicators for the temperature at which sintering may occur. The Hüttig ($T_{\text{Hüttig}} = 0.3T_{\text{melting}}$) and Tamman ($T_{\text{Tamman}} = 0.5T_{\text{melting}}$) temperatures are semiempirical and correspond to the expected onset of

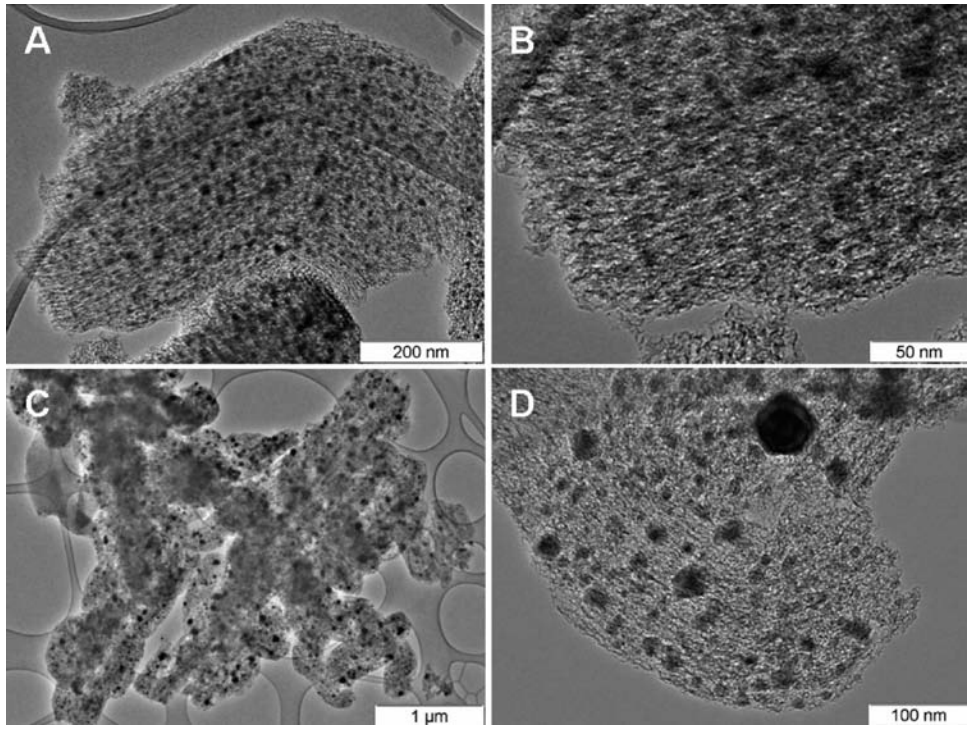

Figure 8. TEM (Hitachi HF 2000) images of C-Fe-2.33-400 after reaction for 16 h at 600 °C (A, B) and 700 °C (C, D).

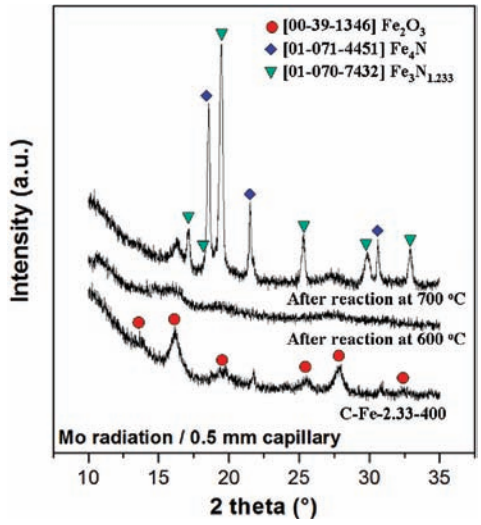

Figure 9. XRD patterns of the C-Fe-2.33-400 catalyst before and after catalytic tests at 600 and 700 °C.

surface diffusion and bulk diffusion, respectively. The melting point of bulk Fe_2O_3 is 1838 K; the corresponding Hüttig ($T_{Hüttig}$) and Tamman (T_{Tamman}) temperatures are thus ca. 613 K (340 °C) and 919 K (646 °C). Since these temperatures are either lower or in the range of the reaction temperatures, it is not surprising that sintering of such small Fe-based nanoparticles occurred, especially, since it has been suggested already 100 years ago and later many times experimentally confirmed that, for small particles, melting points can be strongly decreased.[46]

The XRD patterns of the catalysts before and after reaction are displayed in Figure 9. The samples were packed in a 0.5 mm capillary and then measured with molybdenum radiation in transmission mode. Before reaction, the C-Fe-2.33-400 sample shows broad reflections, which can be assigned to γ-Fe_2O_3 as indicated by the dots. The iron oxide particle size is estimated to 6 nm, based on the Scherrer equation, which is in good agreement with the TEM observations (Figure 2). After ammonia decomposition reaction, the XRD patterns of the catalysts are significantly different from those of the original one. The catalyst reacted at 600 °C has an XRD pattern with only weak detectable reflections. Although the broad reflections occur at the same diffraction angle as those of γ-Fe_2O_3, they cannot be clearly assigned to a defined crystalline phase. The loss of the reflection intensity might be attributed to the formation of other, X-ray amorphous iron species, or fragmentation of the particles into very small crystals. Noticeably, at 600 °C, this catalyst does exhibit long-term stability for ammonia conversion. This reveals that those X-ray amorphous iron species or small crystals are active for ammonia conversion. After reaction at 700 °C, three different crystalline phases including γ-Fe_2O_3, Fe_4N, and $Fe_3N_{1.233}$ are formed. The reflections corresponding to Fe_xN_y phases are very sharp, indicating a particle size larger than 25 nm. This is in agreement with the TEM observation (Figure 8). The XPS analyses reveal that, after reaction at 700 °C, signals corresponding to iron (with high intensity) and nitrogen arise. In comparison with the XPS of C-Fe-2.33-400, the detected iron and nitrogen signals indicate that Fe_xN_y species appeared on the external surface of the carbon support. At 700 °C, the mobility and corresponding sintering of the iron-containing particles are responsible for the deactivation of the catalyst.

Thus, in order to find a solution for retaining the particles on the pore system, the carbon/silica composite was used as the catalyst support where the additional silica layer might provide an additional barrier against movement of the iron species and an additional anchor site for the iron-containing particles.

Figure 10 shows the ammonia conversions over a series of CS-Fe-z-400 catalysts with different Fe-loadings. As shown in Figure 10A, the maximum conversion of CS-Fe-2.33-400 is reached after a short activation period. During this period the ammonia conversion gradually increased and approached a steady conversion after about 1−2 h. Independent of the Fe-loading, a constant conversion is retained even after 20 h in an ammonia stream at 600 °C. No catalyst deactivation was observed for the CS composite catalysts. As expected, with an increase in space velocity, the conversion over the CS-Fe-z-400 catalyst gradually decreased. However, even at a space velocity of 120 000 $cm^3\ g_{cat}^{-1}\ h^{-1}$, still more than 20% of ammonia was converted on CS-Fe-2.33-400 at a temperature

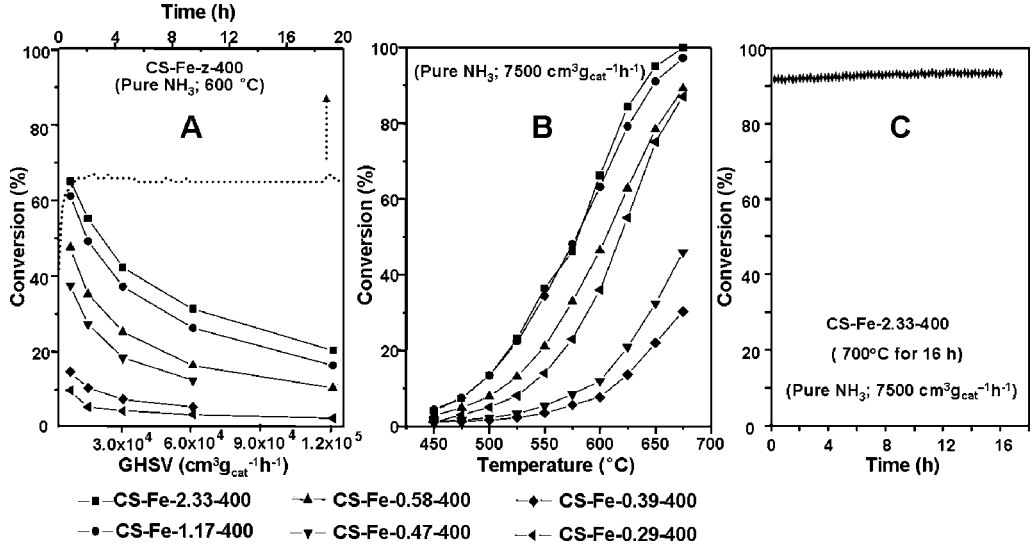

Figure 10. (A) Catalytic activity measured at 600 °C as a function of GHSV for different CS-Fe-z-400 catalysts (dotted line: Catalyst stability at 600 °C and GHSV = 7500 $cm^3\ g_{cat}^{-1}\ h^{-1}$); (B) temperature dependent catalytic activity measured at a GHSV of 7500 $cm^3\ g_{cat}^{-1}\ h^{-1}$; and (C) catalytic stability measured at 700 °C and GHSV = 7500 $cm^3\ g_{cat}^{-1}\ h^{-1}$.

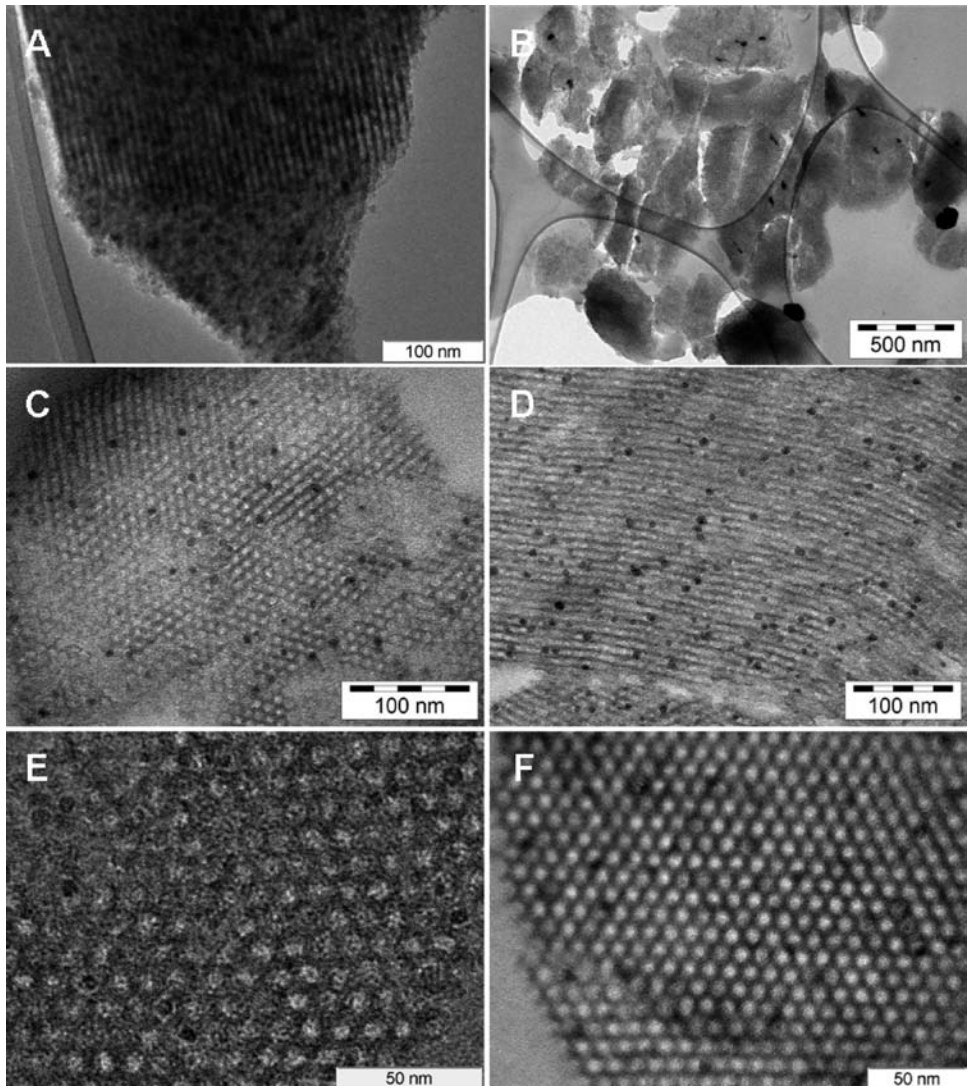

Figure 11. TEM (Hitachi H-7500) images (A, B) of CS-Fe-2.33-400 measured after catalysis test at 600 and 700 °C, respectively, and TEM images from the 60 nm thick microtome sections of the CS-Fe-1.17-400 (C, D) after reaction and CS-Fe-0.58-400 ((E) before reaction; (F) after reaction). Reaction conditions: 600 °C, 20 h, 7500 $cm^3\ g_{cat}^{-1}\ h^{-1}$.

of 600 °C. As seen in Figure 10B, the highest conversion of ammonia was achieved for the catalyst CS-Fe-2.33-400 with 5.1 wt % Fe-loading. At 600 °C and a space velocity of 7500 $cm^3\ g_{cat}^{-1}\ h^{-1}$, more than 65% ammonia was converted to N_2 and H_2. The TEM image in Figure 11A shows that, after reaction at 600 °C, iron-based nanoparticles are still highly dispersed within the CS support; no sintering effect occurs. By increasing the temperature to 675 °C, complete ammonia decomposition was reached. As seen in Figure 10C, a stability test at 700 °C and with a space velocity of 7500 $cm^3\ g_{cat}^{-1}\ h^{-1}$ showed that ca. 93% of ammonia was continuously decomposed over a reaction period of 16 h, and no deactivation was observed. After catalysis, the mass loss of this composite catalyst is ∼20 wt %. The specific surface areas changed from 370 $m^2\ g^{-1}$ before to 420 $m^2\ g^{-1}$ after catalysis. The slight deactivation of this catalyst at 700 °C is due to partial sintering of the iron-based catalyst, as seen in the TEM image in Figure 11B. However, the sintering degree is much less significant than that for the purely carbon supported catalyst C-Fe-2.33-400 (Figure 8C, D). Though there are some particles sintered, the EDX analysis result demonstrated that iron species are still highly dispersed in the matrix. This indicates that the carbon-silica support stabilizes the dispersion of the nanosized iron catalyst better than pure carbon. A clear correlation between Fe-loading and catalytic activity exists; i.e. catalytic activity increases with an increasing concentration of iron.

In order to check the importance of the carbon in the system, an iron oxide catalyst supported on SBA-15 was measured as reference. While, for catalyst CS-Fe-1.17-400 with 2.5 wt % Fe-loading, more than 60% ammonia was decomposed at 600 °C and a space velocity of 7500 $cm^3\ g_{cat}^{-1}\ h^{-1}$, pure SBA-15 with 2.4 wt % converted only ∼21% of ammonia under the same conditions. Clearly, a carbon layer coated on the mesopore walls of SBA-15 is important for achieving a high catalytic activity.

(41) Süzer, S. *Appl. Spectrosc.* **2000**, *54*, 1716.
(42) Chen, W.; Fan, Z.; Pan, X.; Bao, X. *J. Am. Chem. Soc.* **2008**, *130*, 9414.
(43) Pan, X.; Fan, Z.; Chen, W.; Ding, Y.; Luo, H.; Bao, X. *Nat. Mater.* **2007**, *6*, 507.
(44) Zhang, J.; Comotti, M.; Schüth, F.; Schlögl, R.; Su, D. S. *Chem. Commun.* **2007**, 1916.
(45) Kleine, A.; Ryder, P. L.; Jaeger, N.; Schulz-Ekloff, G. *J. Chem. Soc., Faraday Trans. 1* **1986**, *82*, 205.
(46) Pawlow, P. *Z. Phys. Chem.* **1909**, *65*, 545.

The nanostructures of the Fe_2O_3/CS catalysts were investigated by TEM. Figure 11C, B show the morphologies of CS-Fe-1.17-400 with 2.5 wt % Fe-loading after exposure to an ammonia stream at 600 °C for 20 h. The hexagonally ordered pore structure of the support was retained after reaction. The dark spots correspond to the Fe-containing nanoparticles. The image taken perpendicular to the mesopore channels (Figure 11D) shows Fe-containing nanoparticles homogeneously distributed throughout the entire support; no aggregated big particles were observed. The nanoparticles are mainly present in the form of nearly spherical particles with diameters of around 6 nm. This indicates that the Fe-based nanoparticles are firmly anchored on the pore walls.

Figure 11E, F shows TEM images of CS-Fe-0.58-400 with 1.4 wt % Fe-loading before and after the catalytic test. Obviously, the images of the material before and after catalysis are rather similar. After reaction, the nanoparticles are still homogeneously distributed in the CS support. No bigger particles are visible in the TEM images, indicating that no sintering of the iron species took place. However, on closer inspection, it can be seen that the shape and the position of the nanoparticles have changed. The particles are not any longer located inside the mesopores, but embedded in the pore walls of the composite support for which they had to penetrate the thin carbon layer cladding the silica walls. Thus, the Fe-based particles are anchored on the silica walls. Consequently, these nanoparticles are better protected against migration to the external surface of the support where they could form big particles. Thus, with the carbon-silica composites as catalyst supports, catalysts with high stability in ammonia decomposition can be synthesized.

4. Conclusions

Highly dispersed γ-Fe_2O_3 ($\sim$6 nm) exclusively immobilized within the intrapore channels of CMK-5 can be prepared simply by wet impregnation and thermal treatment under argon of the initial SBA-15 silica in which the inside of the channels is coated with a thin carbon layer. An additional pore system can be opened by leaching of the silica from the precursor. This provides a blueprint for the controlled functionalization of the two pore systems by different means. Due to the large pore volume of CMK-5, high Fe-loadings of up to about 12 wt % can be achieved with a single impregnation step.

Using such catalysts, complete ammonia conversion can be realized at 600 °C at a space velocity of 7500 $cm^3\ g_{cat}^{-1}\ h^{-1}$, and full conversion was retained for 16 h without any deactivation. With a higher space velocity of up to 60 000 $cm^3\ g_{cat}^{-1}\ h^{-1}$, complete ammonia decomposition can be achieved at 700 °C. This is the best reported catalytic activity for Fe-based catalysts in this reaction. The high activity of Fe_2O_3/CMK-5 catalysts is possibly due to the high porosity of the CMK-5 support, which is beneficial for the mass transfer, and the high dispersion of the iron oxide.

Under reaction conditions at 700 °C, some sintering and migration of large particles to the external surface of the CMK-5 support takes place. In order to prepare structurally more stable catalysts, Fe_2O_3 nanoparticles were immobilized within the channels of the carbon/SBA-15 composite. This stabilizes the dispersion of the iron oxide on the silica walls, because the iron oxide particle penetrate the thin carbon layer and are then immobilized more strongly on the silica surface, while still retaining some contact with the carbon, as the higher catalytic activity compared to pure SBA-15 suggests.

Acknowledgment. The authors would like to thank the MPS project ENERCHEM. We thank Mr. Spliethoff, Mr. Dreier, and Mr. Bongard for measuring TEM and SEM, and Mr. Mienert and Dr. Bill for measuring Mössbauer spectra (Max-Planck-Institut für Bioinorganic Chemistry). A.H.L. would like to thank the Fundamental Research Funds for the Central Universities and the Program for New Century Excellent Talents in University of China (NECT-09-0254).

JA105308E